Available online at www.sciencedirect.com
SCIENCE DIRECT®
ELSEVIER
Nuclear Instruments and Methods in Physics Research A 542 (2005) 134–141
NUCLEAR INSTRUMENTS & METHODS IN PHYSICS RESEARCH Section A
www.elsevier.com/locate/nima

Study of water distribution and transport in a polymer electrolyte fuel cell using neutron imaging

N. Pekula, K. Heller, P.A. Chuang, A. Turhan, M.M. Mench, J.S. Brenizer*, K. Ünlü

Pennsylvania State University, 138, Reber Building, University Park, PA 16803, USA

Available online 19 February 2005

Abstract

A procedure to utilize neutron imaging for the visualization of two-phase flow within an operating polymer electrolyte fuel cell has been developed at the Penn State Breazeale Nuclear Reactor. Neutron images allow us to visualize the liquid water inside the flow channel (~0.5 mm deep) and gas diffusion media (~200 μm thick) in real operating conditions. The current temporal and spatial resolution for radioscopy is approximately 30 frames/s and 129 μm/pixel in a 50 cm^2 image area. Continuous digital radioscopy can be recorded for 45 min. The determination of water volume within the cell has been enabled by referencing a calibration look-up table that correlates neutron attenuation to an equivalent liquid water thickness. It was found that liquid water tends to accumulate at specific locations within the fuel cell, depending on operating conditions. Anode flow channel blockage was observed to occur at low power, while higher power conditions resulted in more dispersed distribution of liquid droplets. Under high-power conditions, liquid water tended to accumulate along or under the channel walls at 180° turns, and radioscopy revealed that individual liquid droplet velocities were several orders of magnitude less than that of the reactant flow, indicating a slug-flow regime up to at least 1 A/cm^2.

PACS: 42.30.Va; 42.79.Pw; 84.60.Dn

Keywords: Fuel cell; Neutron radiography; Water management; Imaging

1. Introduction

Recently, fuel cell technology has gained high interest in stationary, portable, and automotive applications, due to vast improvements in performance, increased environmental concern, as well as a need for petroleum-free power sources. Due to its high efficiency, low operating temperature (~30–80 °C), and rapid evolution over the past decade, the polymer electrolyte fuel cell (PEFC) is currently under intense research and development.

*Corresponding author. Tel.: +1 814 863 6384; fax: +1 814 863 4840.
E-mail address: brenizer@engr.psu.edu (J.S. Brenizer).

0168-9002/$ - see front matter © 2005 Elsevier B.V. All rights reserved.
doi:10.1016/j.nima.2005.01.090

Fig. 1 shows the basic operation of a hydrogen PEFC. Hydrogen is supplied to the anode of the fuel cell while oxygen, usually taken from the air, is supplied to the cathode. The electrochemical oxidation reaction at the anode produces hydrogen ions and electrons.

The flow of the electrons through an external circuit powers a load. The ions produced at the anode are transported through an ionically conductive polymer electrolyte to the cathode, where water is produced. A platinum catalyst layer (~10–20 μm) is typically employed at both electrodes to reduce the activation energy for the electrochemical reactions. Covering each electrode is a 200–400 μm porous carbon fiber gas diffusion layer (GDL). The GDL functions to enable reactant transport to, and product from the catalyst layer, while providing conductivity for electron transport.

The ratio of the theoretical required flow rate and the actual reactant flow rate is known as the gas flow stoichiometry for anode (ξ_a) and cathode (ξ_c), respectively. In order to maintain constant stoichiometry, the flow rate increases with current. It is necessary to operate fuel cells at ξ_a and $\xi_c > 1.0$.

In a PEFC, the level of water must be precisely balanced. Adequate water vapor must be available to maintain high electrolyte ionic conductivity and ensure suitable performance [1,2]. However, if excessive water is present in the liquid phase, it can block pores in the catalyst and GDLs, which hinders the transport of reactants to the catalyst. This phenomenon is known as "flooding", and greatly diminishes cell performance. At a cell operating temperature of 80 °C, a 1 °C change in temperature causes nearly a 5% shift in saturation vapor pressure. Due to the delicate balance between the benefit of saturated flow and the deleterious effects of flooding concomitant with liquid water accumulation, there is extensive ongoing research to more fundamentally understand two-phase water transport in PEFCs, to enable performance and design optimization.

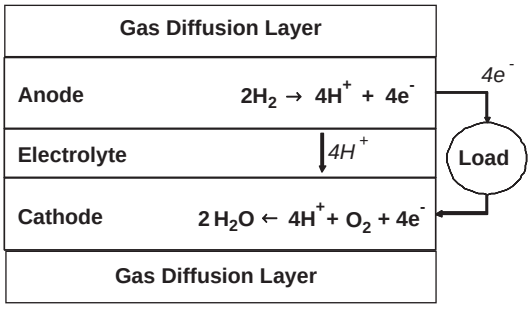

Fig. 1. Simplified Schematic of PEFC.

Although there have been numerous models presented in literature that predict the water production and transport phenomena in fuel cells, there has been little research in experimental visualization and quantification of the liquid water distribution and transport. Neutron radiography and radioscopy are excellent non-intrusive techniques for visualization and quantification of the two-phase flow within the fuel cell in real time or steady-state. Due to the nearly 1000-fold decrease in molecular density between gas and liquid phase water, the gas-phase humidified reactant flow, only liquid water is observable, so that variations in gas-phase humidity typical in PEFCs do not affect imaging results.

2. Experimental setup

The neutron radioscopy system and thermal neutron beam from the Breazeale Nuclear Reactor at the Penn State Radiation Science and Engineering Center was utilized in this study. Specialized image processing hardware was developed for the analysis, storage and presentation of the collected images.

The Penn State Breazeale Nuclear Reactor (PSBR) is located at the Penn State Radiation Science and Engineering Center (RSEC). The pool-type reactor utilizes a Training Research Isotope production General Atomics (TRIGA) core. The core operates at a maximum steady-state power level of 1000 kW. The Neutron Beam Laboratory (NBL) is one of several research facilities located at the PSBR. Using a D_2O tank to thermalize neutrons and a graphite reflector, a well-collimated beam of thermal neutrons is available for transmission to one of seven beam ports located in the facility. At a maximum reactor power level of 1000 kW, the neutron flux at the

port aperture is approximately 3×10^7 neutrons/cm^2 s at an L/D ratio of 140 at the imaging plane [3].

An integrated test station at the NBL was built to control and monitor the fuel cell operating parameters. The NBL Test Station (NBLTS) is isolated from the neutron beam source, as illustrated in Fig. 2. The station can accommodate various sized fuel cells (up to 22.8 cm diameter in a single frame) for neutron-imaging processes, with remotely controlled fuel cell operation.

The fuel cell control system utilizes a Lynntech, Inc. electronic loadbank with a maximum current rating of 1000 A and a maximum voltage rating of 20 V. The system allows for fully user programmable operation of the fuel cell. The anode and the cathode gas flows are controlled by digital mass flow controllers (MKS Technologies, M100B). The NBLTS is also equipped with a nitrogen purge option which allows the operator to exhaust reactant gases from the fuel cell and the test station gas lines at any time. The relative humidity of the reactant gases is controlled through a sparging-type humidification subsystem. The fuel cell operating pressures are individually controlled by back-pressure regulators (Tescom Corp., 44-2361-24), positioned down stream of the cell. Voltage output-pressure transducers (Omega Engineering, PX213-060G5 V) are

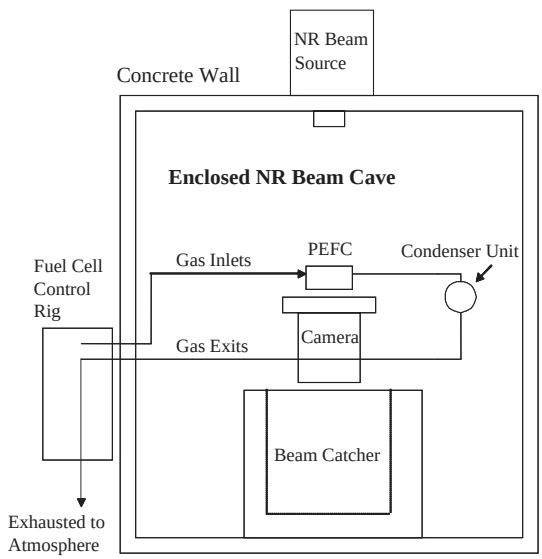

Fig. 2. Test station for fuel cell imaging at the NBL.

capable of measuring and recording the gas flow pressures in real time. All of the temperature processes are managed using PID temperature controllers (Omega, CN9300). Two 6.3 mm diameter cartridge heaters, one in each cell backing plate, provide equal heating to each flow field. The gas flow lines and humidifiers are heated using resistive heat tapes.

Special consideration was taken in the design of the fuel cell components to reduce the overall attenuation and scattering of the neutron beam, while maintaining the same thermal and performance characteristics of a regular PEFC. The graphite flow field plates found in a standard PEFC were replaced with aluminum plates. The aluminum plates were coated with a very thin layer of gold for low contact resistance. The attenuation and scattering of neutrons caused by the gold layer was negligible due to its very small thickness. The cell compression plates and current collectors were also constructed of aluminum (Al Alloy 6061-T6). The thickness of the cell components was reduced to lower beam attenuation.

The platinum catalyst loading for both the anode and cathode was 0.40 mg Pt/cm^2. Toray carbon paper, TP-060 and TP-090, was used for the gas diffusion media for the anode and cathode, respectively. A parallelized serpentine-style pattern was utilized for both the anode (two parallel pass channel configuration) and cathode (three parallel pass).

Both neutron radiography and neutron radioscopy were utilized to observe steady-state and transient behaviors, respectively. The neutron radiography was taken at a reactor power level of 800 kW for 4.5 min using Kodak SR45 film and a gadolinium converter in a vacuum cassette. The best resolution for this procedure allows objects such as liquid water droplets to be discerned in the range of approximately 50–70 μm. The neutron radiography setup only allows for single exposures to be taken. Neutron radioscopy is advantageous over radiography in that the temporal resolution is greatly enhanced allowing for real-time video of the fuel cell to be monitored and recorded. The current temporal and spatial resolution for radioscopy is approximately 30 frames/s and 129 μm/pixel in the 50 cm^2 active area. Continuous digital

radioscopy can be continuously recorded for up to 45 min. The radioscopic flat-fielded images have a single-to-noise ratio of 160.

3. Data acquisition and analysis

A video capturing software program, Streampix, collects and records the fully digital video signal produced by the CCD camera system on a customized computer. The image stacks are stored on a date based directory structure with each stack file name containing a descriptor of the experiment recorded. Each image within the stack is also affixed with a time stamp during acquisition. These features allow single images of interest or multiple sequential images to be easily located and analyzed.

3.1. Image post-processing

Several post-process image enhancement techniques were used to increase the overall image quality and accuracy of the water quantification process. Minor fluctuations in the reactor power level, which is common during experiments, result in changes in the neutron beam flux and consequently the corresponding measured pixel luminance values. Fluctuations are usually minor but can be as high as 1% of the operating reactor power level. By monitoring a reference location on each image that is recorded, the beam intensity between each frame is determined and the entire image is normalized accordingly. The reference is a static location, such as the fuel cell backing plate outside the active area where pixel luminance should be theoretically constant throughout the length of an experiment. This procedure is referred to as Reactor Power Normalization.

The intensity of the neutron beam is not perfectly uniform across the fuel cell image plane. This results in different pixel luminance values even where material attenuation characteristics and thicknesses are identical. By examining a blank image (only the uninterrupted neutron beam), the average pixel luminance value of the entire array is determined. The acquired average value is divided by each individual pixel luminance value of the array to produce a corresponding correction factor for each pixel. The correction factor matrix is then multiplied by each image recorded during actual experiments to produce a ''flattened'' image making the initial beam intensity uniform on the fuel cell. It was assumed that the neutron beam shape is constant for each experiment.

Random noise and noise caused by the analog-to-digital conversion process can cause time varying error. To account for this, the luminance value of corresponding pixels within sequential images can be averaged together. This process improves image quality and makes liquid water accumulation and movement more discernible. Several other image enhancement techniques are possible to improve qualitative analysis and are excellent for the presentation of single images or video. These include false colorization of liquid water in the fuel cell to make it more discernible. In addition, the values of a pixel array of an initial recorded image of a fuel cell containing no water could be divided into those of a water-filled cell. This produces an image of only liquid water in the cell.

3.2. Water quantification

The ability to store individual images digitally allows for easy post-process analysis including ascertaining pixel luminance values within the fuel cell. Consequently, the determination of water content within the cell as a function of time is attainable by referencing a pre-generated calibration look-up table, which correlates water thickness to pixel luminance [4]. The minimum detectable water thickness was measured to be 12.7 μm. This look-up table is generated using a water-filled wedge, constructed of aluminum (Al alloy 6061-T6). The wedge has the exact same through-plane dimensions to duplicate the neutron attenuation and scattering effect of the fuel cell. The wedge is the exact distance from the beam port aperture as the fuel cell to ensure the equal beam intensity and hence measured attenuation as the fuel cell. The wedge contains a water-filled void of continuously varying thickness. The steady and gradual decrease in pixel luminance from the

bottom to top of the wedge is representative of the increasing water thickness level within the wedge. Through statistical analysis of the wedge, pixel luminance values are recorded at the known water thickness levels producing a correlation look-up table. This look-up table can then be referenced to assign water thickness values to individual areas within the cell or the entire cell as a whole. The mass and volume of water in the cell can then be computed for finite instances or as a varying function of time. The quantification of liquid water within the cell is comprised of line-averages of water through the entire fuel cell assembly (i.e., gas flow channels, MEA, and gas diffusion media). A correlation look-up table is generated for each experiment to account for differences in the neutron beam flux and reactor power level between an experimental run. This method works well in this application because the water thickness is at most 1 mm, and they are typically less than 250 μm. Thus, there are essentially no multiple neutron scatters.

4. Neutron radiography results

A series of neutron radiographs were collected using the fuel cell and imaging setup. The current density and gas flow stoichiometries were varied, while the cell temperature (80 °C) and gas flow back pressure (0.274 MPa) were maintained constant throughout the experiments. The relative humidity of the anode and cathode were maintained at 100% at 80 °C for all tests. Between each experiment, the fuel cell was allowed to operate for approximately 1 h at the prescribed test conditions to ensure steady-state had been achieved.

4.1. Water accumulation at low current densities

Fig. 3 shows substantial water accumulation near the fuel cell exit (lower left corner) for radiographs taken at a current density of 0.05 A/cm^2. Note the inlet of the anode and cathode is the upper right, and the exit is at the lower left in all images. The dark areas in the middle of the fuel cell are the anode and cathode cartridge heaters. The images show liquid water occupying a large portion of the gas flow channels causing channel flooding inside the fuel cell. From the flow channel geometry (2-channel pass design on anode and 3-channel design on the cathode) it can be concluded that the liquid water is on the anode side of the cell. This conclusion was validated through real-time radioscopy of the fuel cell at the same operating conditions.

An experiment was conducted to determine the cause of the water accumulation in the anode side gas channels of the fuel cell for these conditions. The fuel cell anode and cathode flow rates were identical to those at 0.05 A/cm^2, but the cell was operated at open circuit to eliminate water production at the cathode and eliminate electro-osmotic drag and diffusion of water between the anode and cathode. The radiographic image of the fuel cell at these conditions showed a similar water accumulation pattern in the anode flow channels, indicating that a majority of the liquid water accumulation in the anode channel under low-power conditions can be attributed to water condensation from the humidified hydrogen gas flow, and not cathode generation or back diffusion. The condensation of water almost completely blocks the gas flow channel. This is a result of the inability to remove water via viscous drag with the extremely low anode flow rate (23 sccm) required for 0.05 A/cm^2.

4.2. Water accumulation at high current densities

Fig. 4a, b, and c show three separate radiographs at a current density of 1.0 A/cm^2 and cathode stoichiometries (ξ_c) at 2.0, 1.4, and 1.3, respectively. The images show that highly dispersed liquid droplets are present in the lower half of the fuel cell, and that the flow channels near the cell inlet (upper portion) contain almost no liquid water at all. This is most likely due to the water vapor being continually added to the gas flow stream along the flow channel path via generation until saturation. Local temperature increase due to reaction inefficiency, and decreasing pressure along the flow paths allow the initially saturated flows to uptake some of the additional water vapor created by electrochemical reaction. Similar results were seen in radiographs taken at current densities

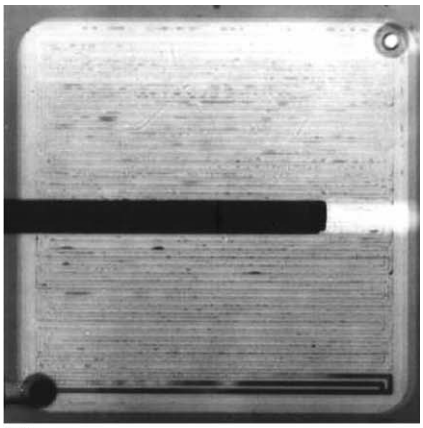

(a)

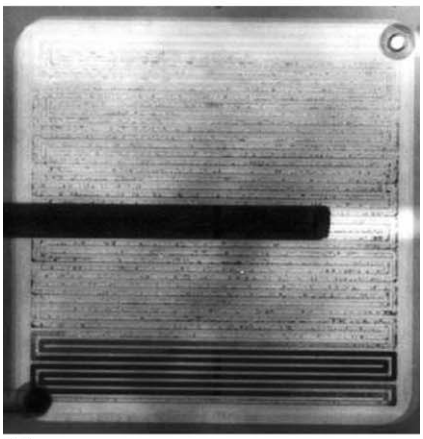

(b)

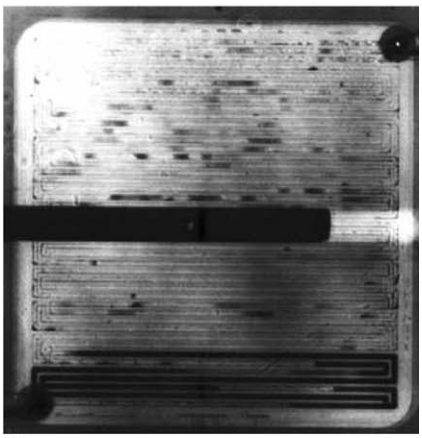

(c)

Fig. 3. Neutron radiographs for (a) $\xi_c = 10.0$; 2.5 A; 0.843 V, (b) $\xi_c = 6.5$; 50 A; 0.857 V, (c) $\xi_c = 6.0$; 2.5 A; 0.868 V.

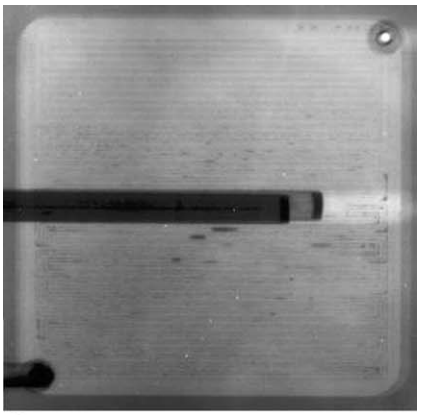

(a)

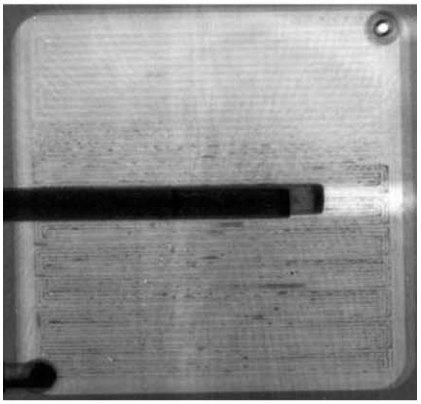

(b)

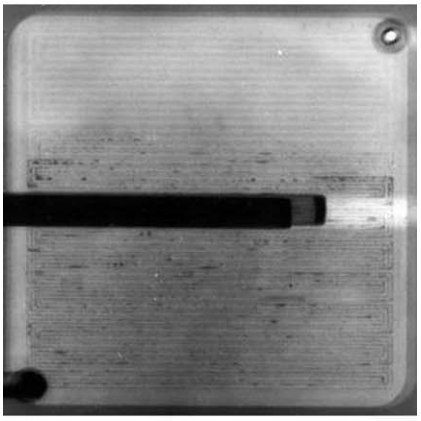

(c)

Fig. 4. Images of neutron radiography for (a) $\xi_c = 2.0$; 50 A; 0.725 V, (b) $\xi_c = 1.4$; 50 A; 0.625 V, (c) $\xi_c = 1.3$; 50 A; 0.600 V.

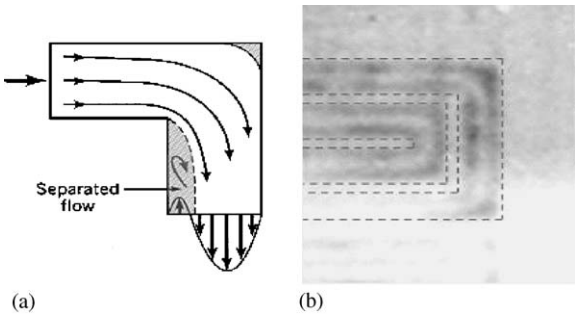

Fig. 5. (a) Illustration of flow in a 90° bend [7] and (b) magnified images showing stratified water accumulation.

of 0.5 A/cm^2. The increase in liquid water saturation along the flow channel path, as well as increased saturation with lower gas flow velocities, is consistent with existing two-phase flow models pertaining to PEFCs in Refs. [5,6].

The radiographs shown in Fig. 4, along with other data not shown, illustrate that liquid water tends to accumulate at particular locations within the fuel cell. These specific areas include the 90° and 180° turns in the gas flow channels near the edges of the cell active area. This may be due to the change of momentum in the gas flow at these locations resulting in localized pressure variations. In addition, liquid water may accumulate due to the decrease in gas flow velocity at the walls and corners of the channels, similar to an annular flow regime. Fig. 5a illustrates the flow character in a typical 90° bend [7]. The accompanying image, Fig. 5b, is a magnified portion of flow channels of Fig. 4a, illustrating water accumulation on or under and adjacent to the gas channel walls. The dashed lines were added to represent the flow channel walls.

5. Real-time neutron radioscopy results

Real-time (30 fps) neutron radioscopy video of the operating fuel cell was recorded for a wide variety of test conditions. Video was recorded for approximately 20 minute for each experiment. The high temporal resolution of the radioscopy procedure allowed for the liquid water accumulation and transport in the cell to be directly observed. Further image analysis gave insight into the characteristics of the liquid water droplet behavior and flow velocities.

The frequency at which liquid water droplets were removed from the cell increased with increasing gas flow rates, as expected. For current densities of 0.5 and 1.0 A/cm^2, the movements of water droplets in the fuel cell were much more frequent and visible as compared to lower operating loads, due to the higher gas flow velocities. A cyclic pattern of water accumulation followed by water removal from the cell was observed for these conditions when examined over periods of several minutes. It was observed that individual droplets clearly accumulated in the gas flow channels of the fuel cell until a critical volume was reached and the induced shearing force of the flow overcame the surface tension between the droplet and the flow channel or gas diffusion media surface.

Sequential images were examined to investigate the behavior of individual water droplets within the cell. Droplets tend to develop and accumulate until a critical volume is reached, and the viscous drag forces imposed by the flow overcome the surface tension between the droplet and channel wall and GDL surface. Following the initial movement, it is quite clear the droplet does not maintain a constant shape or size, but changes based on its interactions with the flow channels and other droplets. As it travels along the flow path, it is quite common for the droplet to amalgamate with others and/or initiate movement of the other droplets in its path. It was observed that under moderate-to-high current density conditions (0.5–1.0 A/cm^2), a single initial moving droplet is most commonly the main impetus for significant water removal. In addition, the velocity of a moving droplet is very unsteady, most likely due to changes in its shape and size. Additionally, moving droplets periodically stop completely and then often begin moving again. The velocities of water droplets in the cell were measured for several operating conditions. For a current density of 0.5 A/cm^2 and an anode stoichiometry of 3.0 (573 sccm), the average velocities of the particular droplets under examination ranged from 7.7 to 13.45 cm/s. The gas flow velocity on the anode for this analysis was 418 cm/s. For a current density of

1.0 A/cm^2 and an anode flow velocity of 836 cm/s, a droplet velocity was measured to be 53.5 cm/s. This indicates that the droplet velocity cannot be assumed to be on the same order of magnitude as the gas flow velocity for the fuel cell configuration and conditions tested, and a homogeneous, no-slip model of the two-phase channel flow is inappropriate for channel level two-phase modeling.

6. Conclusions

Neutron radiography and radioscopy yield excellent spatial and temporal resolution for the investigation of water transport phenomenon and the measurement of liquid water inside an operating polymer electrolyte fuel cell. The results showed that for various operating conditions, liquid water had a tendency to accumulate at specific locations within the fuel cell, most notably at 90° bends in the gas flow channels. For low current densities of 0.05 A/cm^2, it was shown that a significant amount of liquid water accumulated in the anode gas channel. At higher current densities of 0.5 and 1.0 A/cm^2, dispersed liquid droplets were observed in the final 2/3 of the flow path with channel wall accumulation at turns in the flow field. It was also shown that channel-level liquid droplet velocity is not constant, and changes substantially due to interactions with the flow channel walls and other droplets. The maximum velocity of the droplets is an order of magnitude less than the reactant gas flow. For the fuel cell configuration and conditions tested, a slug-flow model of two-phase flow in the gas channels is appropriate up to at least 1 A/cm^2.

References

[1] J. Larminie, A. Dicks, Fuel Cell Systems Explained, Wiley, West Sussex, England, 2000, pp. 61–107.
[2] T.E. Springer, T.A. Zawodzinski, S. Gottesfeld, J. Electrochem. Soc. 138 (8) (1991) 2334.
[3] C.F. Sears, K. Ünlü, T.L. Flinchbaugh, S.K. Ripka, A.D. Pope, 48th Annual Progress Report, Penn State Radiation Science & Engineering Center, 2003.
[4] J.S. Brenizer, K.W. Tobin, J.M. Hylko, D.D. McRae, R.W. Jenkins Jr., Mater. Eval. 45 (1987) 1310.
[5] Z.H. Wang, C.Y. Wang, K.S. Chen, J. Power Sources 94 (2001) 40.
[6] L. You, H. Liu, Int. J. Heat Mass Transfer 45 (2002) 2277.
[7] B.R. Munson, D.F. Young, O.H. Theodore, Fundamental of Fluid Mechanics, Wiley, New York City, 1998, pp. 496–505.